nature immunology

Direction of leukocyte polarization and migration by the phosphoinositide-transfer protein TIPE2

Svetlana A Fayngerts[1,3], Zhaojun Wang[1–3], Ali Zamani[1], Honghong Sun[1], Amanda E Boggs[1], Thomas P Porturas[1], Weidong Xie[1], Mei Lin[1], Terry Cathopoulis[1], Jason R Goldsmith[1], Anastassios Vourekas[1] & Youhai H Chen[1]

The polarization of leukocytes toward chemoattractants is essential for the directed migration (chemotaxis) of leukocytes. How leukocytes acquire polarity after encountering chemical gradients is not well understood. We found here that leukocyte polarity was generated by TIPE2 (TNFAIP8L2), a transfer protein for phosphoinositide second messengers. TIPE2 functioned as a local enhancer of phosphoinositide-dependent signaling and cytoskeleton remodeling, which promoted leading-edge formation. Conversely, TIPE2 acted as an inhibitor of the GTPase Rac, which promoted trailing-edge polarization. Consequently, TIPE2-deficient leukocytes were defective in polarization and chemotaxis, and TIPE2-deficient mice were resistant to leukocyte-mediated neural inflammation. Thus, the leukocyte polarizer is a dual-role phosphoinositide-transfer protein and represents a potential therapeutic target for the treatment of inflammatory diseases.

Leukocytes, like all eukaryotic cells, sense the presence of chemical attractants (chemoattractants) mainly through chemotactic receptors of the G-protein-coupled receptor (GPCR) family. After binding to chemoattractants, GPCRs activate several intracellular signaling cascades via their associated G proteins, which leads to substantial morphological and biochemical transformation, called 'polarization'[1]. The front pole (leading edge) of a polarized leukocyte is characterized by dynamic remodeling of actin that generates the protrusive structure and the forward-moving force. The rear pole (trailing edge) has only a limited amount of stable filamentous actin (F-actin, or polymerized actin) that facilitates myosin-dependent retraction of cells. This morphological polarity is determined by the asymmetrical activation of proteins such as phosphoinositide 3-OH kinases (PI(3)Ks), the GTPase Rac and actin-regulatory proteins at the leading and trailing edges[1–3]. How GPCR-generated signals direct and steer cells along chemoattractant gradients (as shallow as 2%) is not well understood. Several computational models have been proposed to address this issue. It is predicted that both enhancers and inhibitors of signaling transduction and actin dynamics are required for leukocyte polarization and chemotaxis[1,4–6]. The enhancers operate locally at the leading edge, whereas the inhibitors function globally. However, the nature of these regulators remains to be characterized[1,4–6].

The mammalian TIPE family ('TNFAIP8 ('tumor necrosis factor-α-induced protein 8')-like' (TNFAIP8L)) consists of four proteins: TNFAIP8, TIPE1 (TNFAIP8L1), TIPE2 (TNFAIP8L2) and TIPE3 (TNFAIP8L3). TIPE proteins are risk factors for both inflammation and cancer[7–9], and their expression is dysregulated in various human diseases[10–16]. They share a highly conserved TIPE2 homology domain, which is a barrel-like fold with a lipophilic central cavity[10,17]. All TIPE proteins can bind phosphoinositide species such as phosphatidylinositol 4,5-bisphosphate (PtdIns(4,5)P_2) and phosphatidylinositol 3,4,5-trisphosphate (PtdIns(3,4,5)P_3)[10]. TIPE3 can function as a PtdIns(4,5)P_2-transfer protein; i.e., it can extract PtdIns(4,5)P_2 from the lipid bilayer, accommodate the acyl chains of this lipid in the cavity and shuttle it through the aqueous solutions. This action of TIPE3 promotes the phosphorylation of PtdIns(4,5)P_2 by PI(3)Ks[10]. However, it is not clear if all members of the TIPE family are able to function as PtdIns(4,5)P_2-transfer proteins. In addition to interacting with phosphoinositides, TIPE2 can also directly bind and inhibit Rac[18]. TIPE2 is expressed mainly by bone-marrow-derived cells and suppresses Toll-like-receptor signaling through its interaction with Rac[18,19]. As a consequence, TIPE2-deficient cells are hyper-responsive to activation via Toll-like receptors and have enhanced phagocytic and bactericidal activities, and TIPE2-deficient mice are hypersensitive to intravenously induced septic shock and are resistant to intravenous bacterial infection[18,19].

RESULTS

Defective chemotaxis of TIPE2-deficient leukocytes

To understand the role of TIPE2 in chemotaxis, we studied the migration of circulating leukocytes in the peritoneal cavity of mice deficient in TIPE2 (*Tnfaip8l2*$^{-/-}$; called '*Tipe2*$^{-/-}$' here) and wild-type mice in a mouse model of acute peritonitis. Significantly fewer TIPE2-deficient Ly6G$^+$ myeloid cells than wild-type Ly6G$^+$ myeloid cells migrated into the peritoneal cavity, which left many more TIPE2-deficient myeloid cells than wild-type myeloid cells in the blood of the same mouse (**Fig. 1a**). To study TIPE2-dependent chemotaxis *in vitro*, we used Transwell chambers (for transmigration) and μ-slides

[1]Department of Pathology and Laboratory Medicine, Perelman School of Medicine, University of Pennsylvania, Philadelphia, Pennsylvania, USA. [2]Department of Immunology and Microbiology, School of Medicine, Shanghai Jiao Tong University, Shanghai, China. [3]These authors contributed equally to this work. Correspondence should be addressed to Y.H.C. (yhc@pennmedicine.upenn.edu).

Received 7 February; accepted 3 October; published online 23 October 2017; doi:10.1038/ni.3866

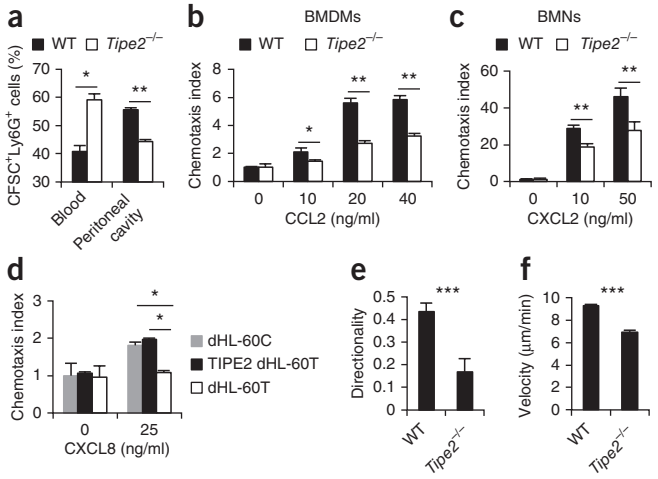

Figure 1 TIPE2 promotes leukocyte chemotaxis both *in vivo* and *in vitro*. (**a**) Frequency (as assessed by flow cytometry) of injected wild-type (WT) and *Tipe2*$^{-/-}$ Ly6G^{+} cells (key) among cells obtained from the blood and peritoneal cavity (horizontal axis) of wild-type mice with acute peritonitis at 16 h after intravenous injection of *Tipe2*$^{-/-}$ (CD45.2^{+}) and wild-type (CD45.1^{+}) bone marrow cells labeled with the division-tracking dye CFSE and mixed at a ratio of 1:1. (**b**–**d**) Chemotaxis index of wild-type and *Tipe2*$^{-/-}$ BMDMs (**b**), wild-type and *Tipe2*$^{-/-}$ BMNs (**c**) and wild-type control dHL-60 (dHL-60C) or dHL-60T neutrophils or TIPE2-expressing dHL-60T neutrophils (TIPE2 dHL-60T) (**d**) during migration through Transwell filters toward CCL2 (**b**), CXCL2 (**c**) or CXCL8 (**d**). (**e**,**f**) Directionality (**e**) and velocity (**f**) of wild-type and *Tipe2*$^{-/-}$ blood neutrophils during migration toward CXCL1 (200 ng/ml) on μ-slides. $^{*}P < 0.05$, $^{**}P < 0.01$ and $^{***}P < 0.001$ (paired Student *t*-test (**a**) or unpaired Student *t*-test (**b**–**d**,**f**) or Mann-Whitney *U*0test (**e**)). Data are representative of two experiments with $n = 5$ mice (**a**; mean + s.e.m.) or are pooled from three independent experiments done in duplicate (technical replicates), with $n = 3$ mice per genotype in **b**,**c** (**b**–**d**; mean + s.d.), or are from one experiment representative of at least three experiments with $n \geq 145$ cells per group (**e**,**f**; mean + s.e.m.).

(for two-dimensional chemotaxis). Bone-marrow-derived macrophages (BMDMs) and bone marrow neutrophils (BMNs) from *Tipe2*$^{-/-}$ mice, as well as human differentiated, TIPE2-deficient HL-60 neutrophils (dHL-60T cells), all showed significant defects in migration through Transwell filters, following chemoattractant gradients, but did not exhibit any defect in random migration relative to that of their wild-type counterparts (**Fig. 1b**–**d** and **Supplementary Fig. 1a**). The chemotaxis defect of dHL-60T cells was fully 'rescued' by the expression of a wild-type *TIPE2* transgene (**Fig. 1d** and **Supplementary Fig. 1a**). Notably, in the μ-slide chemotaxis assay, *Tipe2*$^{-/-}$ neutrophils showed a significant reduction in both directionality (by ~62%) and velocity (by ~25%), relative to that of wild-type cells (**Fig. 1e**,**f** and **Supplementary Fig. 1b**,**c**). Together these results indicated that TIPE2 controlled leukocyte chemotaxis *in vivo* and *in vitro*.

Loss of polarization in TIPE2-deficient leukocytes

To explore how TIPE2 controls chemotaxis, we studied the polarization of neutrophils in response to point-source chemoattractants. To visualize polarization, we expressed in cells a PtdIns(3,4,5)P_3-specific probe (the GRP1-PH domain) tagged with enhanced green fluorescent protein (eGFP) or stained cells for F-actin, Rac-GTP (the active form of Rac) or the AKT phosphorylated at Thr308 (p-AKT(T308)), the active form of AKT that serves as an indicator of activation by PI(3)K[2,3]. By time-lapse microscopy, we compared polarization of wild-type and TIPE2-deficient dHL-60 neutrophils in response to point-source stimulation with the chemokine CXCL8 over a period of 400 s. CXCL8-induced polarization of wild-type dHL-60 cells (which served as the control (dHL-60C cells)) occurred almost immediately after chemokine exposure, with more than 60% of cells polarized 180 s later (**Fig. 2a** and **Supplementary Fig. 1d**). Chemokine-induced polarization was much lower in dHL-60T neutrophils, with only <14% of cells polarized at the end of the observation period.

Similarly, 150 s after exposure to chemoattractants, the vast majority of wild-type BMNs were polarized, with F-actin, Rac-GTP and p-AKT(T308) localized mainly at the leading edge of cells; in contrast, most *Tipe2*$^{-/-}$ BMNs were not polarized (**Fig. 2b**–**g** and **Supplementary Fig. 2a**–**e**). Notably, the polarization defect of dHL-60T neutrophils was 'rescued' by expression of a wild-type *TIPE2* transgene (**Supplementary Fig. 2f**–**h**). TIPE2-deficient cells were sensitive to chemoattractant stimulation, as indicated by their elevated global abundance of p-AKT(T308) and F-actin (**Fig. 2b**,**d**,**f**, **Supplementary Note** and **Supplementary Figs. 2**–**4**). In addition, in response to chemoattractant stimulation, *Tipe2*$^{-/-}$ BMNs increased their spreading areas more significantly than did wild-type BMNs, but they failed to acquire the elongated shape that wild-type BMNs acquired (**Fig. 3a**). Together these results indicated that TIPE2 controlled the stable polarization of the signaling and actin-regulatory molecules essential for formation of the leading and trailing edges in neutrophils moving by chemotaxis.

TIPE2 and Rac in leukocyte polarization

Proteins that inhibit chemoattractant-induced signaling and cytoskeletal activities are predicted to be essential for cell polarization and chemotaxis[1,4–6]. Consistent with published results[18], TIPE2 interacted with Rac in several cell types (**Fig. 3b**–**d** and **Supplementary Note**). We hypothesized that TIPE2-dependent inhibition of Rac was required for effective cell polarization[20]. Pretreatment of *Tipe2*$^{-/-}$ BMNs with the Rac-specific inhibitor NSC24766 before chemokine stimulation significantly reduced cell spreading and abolished the difference between wild-type BMNs and *Tipe2*$^{-/-}$ BMNs in spreading area (**Fig. 3a**). In contrast, the PI(3)K inhibitor LY294002 did not have the same effect on cell spreading (**Fig. 3a**), which suggested that TIPE2 controlled cell spreading through its interaction with Rac. Notably, inhibition of Rac partially 'rescued' the polarization defect of *Tipe2*$^{-/-}$ BMNs and dHL-60T cells: F-actin and p-AKT(T308) were excluded from the edges of the cells opposite the source of the chemoattractants (**Fig. 3e**–**h** and **Supplementary Fig. 5a**,**b**). Thus, TIPE2 served as a cellular inhibitor of Rac, promoting trailing-edge formation and suppressing the generation of secondary leading edges. However, *Tipe2*$^{-/-}$ BMNs and dHL-60T neutrophils treated with the Rac inhibitor failed to form well-defined leading edges (**Fig. 3e**,**f** and **Supplementary Fig. 5b**), suggestive of a Rac-GTP-independent role for TIPE2 in leading-edge formation. Notably, TIPE2 exhibited polarized localization in migrating BMNs, dHL-60C cells and TIPE2-expressing dHL-60T cells: the leading edge showed enrichment for TIPE2, although it was also present throughout the cells (**Fig. 4a** and **Supplementary Fig. 5c**). Since the interaction of TIPE2 with Rac took place in both the cytoplasm and plasma membrane, we sought to determine whether Rac-GTP, localized exclusively at the leading edge, was responsible for the polarized localization of TIPE2. Inhibition of Rac did not significantly change the localization of TIPE2 (**Fig. 4a**,**b** and **Supplementary Fig. 5b**,**c**). However, pretreatment of wild-type BMNs, dHL-60C cells and TIPE2-expressing dHL-60T cells with an inhibitor of PI(3)K abolished the polarized distribution of TIPE2 and F-actin (**Fig. 4a**,**c**–**f** and **Supplementary Fig. 5c**,**d**). In contrast, the

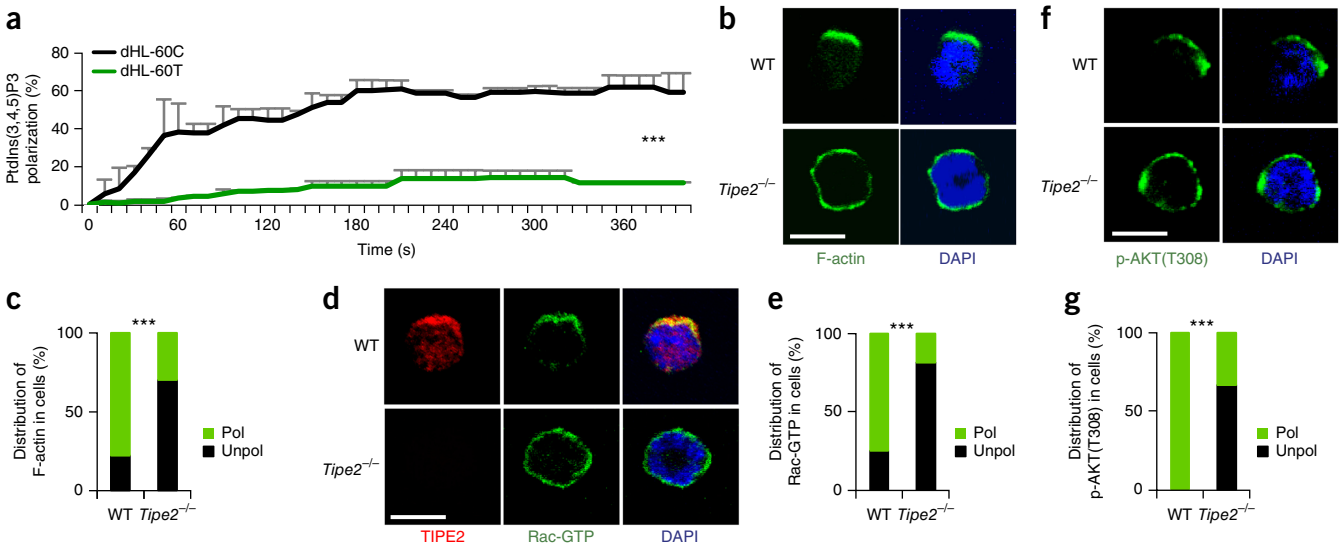

Figure 2 TIPE2 is required for chemoattractant-induced polarization of leukocytes. (**a**) Distribution of PtdIns(3,4,5)P_3 in dHL-60C and dHL-60T neutrophils (key) subjected to point-source stimulation with CXCL8 over 0–400 s (horizontal axis), assessed by time-lapse confocal microscopy, probed with eGFP-GRP1-PH domain, and presented as the degree of polarization of PtdIns(3,4,5)P_3. (**b**–**g**) Confocal microscopy of F-actin (**b**), TIPE2 and Rac-GTP (**d**) or p-AKT(T308) (**f**), as well as the DNA-binding dye DAPI (colors of labels below images indicate color of molecule (or dye) in image), in wild-type and *Tipe2*$^{-/-}$ BMNs (left margin) subjected to point-source stimulation with CXCL8 (**b**,**d**,**f**), and frequency of such cells with polarized (Pol) or unpolarized (Unpol) distribution (key) of F-actin (**c**), Rac-GTP (**e**) or p-AKT(T308) (**g**). Scale bars (**b**,**d**,**f**), 5 μm. ***$P < 0.001$ (Mann-Whitney *U*-test (**a**) or χ^2 test (**c**,**e**,**g**)). Data are pooled from two experiments with $n \geq 45$ cells per group (**a**; mean + s.d.) or three experiments with $n \geq 30$ cells per genotype (**c**,**e**,**g**) or are representative of three experiments with $n \geq 30$ cells per genotype (**b**,**d**,**f**).

inhibitor of PI(3)K altered the distribution of Rac-GTP only slightly: the leading edge showed enrichment for Rac-GTP, but it was also detected at the trailing edge in small amounts (**Fig. 4a**,**c**,**e**). These data suggested that Rac-independent but PI(3)K-dependent mechanisms were probably responsible for the polarized localization of TIPE2 in migrating cells. Together our results indicated that TIPE2 might serve dual roles in the polarization of migrating cells: it controlled trailing-edge formation through inhibition of Rac, and used its Rac-independent and PI(3)K-dependent activities for formation of the leading edge.

TIPE2-mediated transfer of PtdIns(4,5)P_2

To explore the Rac-independent actions of TIPE2 at leading edges, we investigated the functional importance of the binding of TIPE2 to phosphoinositides. We hypothesized that TIPE2 might act differently at membranes containing PtdIns(4,5)P_2 versus those containing PtdIns(4,5)P_2 plus PtdIns(3,4,5)P_3, which are characteristics of trailing edges versus leading edges, respectively. Using small unilamellar vesicles (SUVs) made of phospholipid bilayers, we found that TIPE2 bound effectively to SUVs containing 10% PtdIns(4,5)P_2 (with ~65% of the TIPE2 bound to the vesicle) and, to a lesser extent, to SUVs containing 10% PtdIns(3,4,5)P_3 (with ~14% of the TIPE2 bound), but it bound only very weakly to SUVs containing both 10% PtdIns(4,5)P_2 and 10% PtdIns(3,4,5)P_3 (with ~4% of the TIPE2 bound) (**Fig. 5a** and **Supplementary Fig. 6a**). Consistent with those findings, TIPE2 showed less binding to SUVs containing 5% PtdIns(4,5)P_2 and 5% PtdIns(3,4,5)P_3 than to SUVs containing 10% PtdIns(4,5)P_2 (**Fig. 5a**). TIPE2 did not bind to SUVs containing PtdIns(4)P or only phosphatidylcholine (**Fig. 5a**). Therefore, TIPE2 exhibited differential binding to SUVs containing PtdIns(4,5)P_2 or PtdIns(3,4,5)P_3 or both. Positively charged residues of the α0 helix of TIPE3 mediate the formation of electrostatic interactions with the negatively charged phosphate groups of phosphoinositides[10]. To evaluate whether positively charged residues of the α0 helix of TIPE2 contributed to this protein's interaction with phosphoinositides, we generated mutant TIPE2 in which lysine residues at positions 15 and 16 in the α0 helix were replaced with glutamine (15/16Q) (**Supplementary Fig. 6b**). Similar to TIPE2, 15/16Q bound strongly to SUVs containing 10% PtdIns(4,5)P_2 (**Fig. 5a** and **Supplementary Fig. 6a**). However, this mutant almost completely lost its ability to bind to SUVs containing 10% PtdIns(3,4,5)P_3 (**Fig. 5a**). In addition, 15/16Q was able to interact with PtdIns(4)P-containing SUVs (**Fig. 5a**). To determine to what degree the α0 helix contributed to the binding of TIPE2 to phosphoinositides, we fused eGFP to the wild-type TIPE2 α0 helix or to 15/16Q. We found that the TIPE2 α0 helix interacted with phosphoinositide-containing SUVs with the following order of 'preference', PtdIns(3,4,5)P_3 > PtdIns(4,5)P_2 > PtdIns(4)P, and that replacement of lysine residues within the α0 helix (15/16Q) abolished this interaction (**Fig. 5b** and **Supplementary Fig. 6a**). Notably, unlike PtdIns(4,5)P_2, which showed much less binding to the α0 helix than to full-length TIPE2, PtdIns(3,4,5)P_3 showed binding to the helix that was similar to its binding to full-length TIPE2 (**Supplementary Fig. 6c**). These results suggested that TIPE2 interacted with PtdIns(3,4,5)P_3 but not with PtdIns(4,5)P_2, mostly through electrostatic interactions formed between positively charged amino acids of its α0 helix and negatively charged phosphate groups of the phosphoinositide.

We sought to determine whether the marked reduction in the binding of TIPE2 to SUVs containing both PtdIns(4,5)P_2 and PtdIns(3,4,5)P_3 resulted from PtdIns(3,4,5)P_3-dependant extraction of PtdIns(4,5)P_2 by TIPE2 from the vesicles. We hypothesized that the α0 helix of TIPE2 functioned as a flexible lid of its hydrophobic cavity and that the conformational change induced by the binding to PtdIns(3,4,5)P_3 displaced the lid and allowed TIPE2 to extract PtdIns(4,5)P_2 from the lipid bilayer and transfer it to the solution[10,21]. Indeed, TIPE2 extracted and transferred PtdIns(4,5)P_2 from SUVs

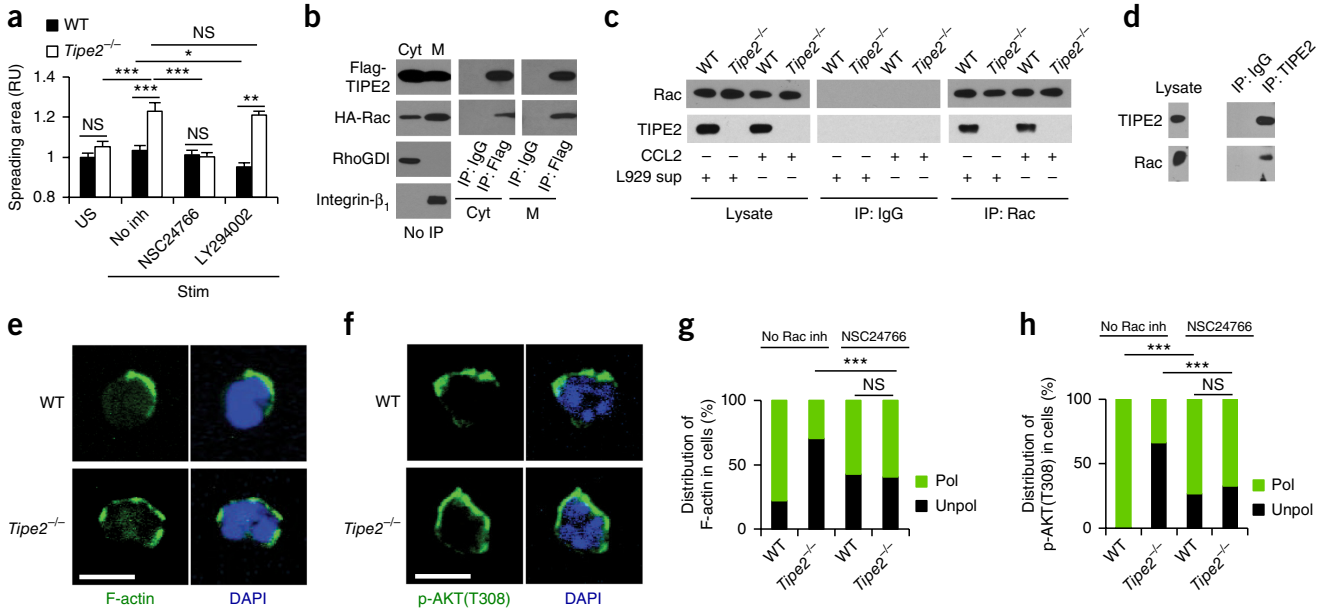

Figure 3 Rac-dependent functions of TIPE2 in cells undergoing chemotaxis. (**a**) Spreading area of wild-type and *Tipe2*$^{-/-}$ BMNs (key) left unstimulated (US) or stimulated (Stim) with CXCL8 from a point source, with or without (No inh) pretreatment with the Rac inhibitor NSC24766 or PI(3)K inhibitor LY294002 (horizontal axis), presented in relative units (RU), relative to results obtained for unstimulated wild-type cells, set as 1. (**b**) Immunoblot analysis of TIPE2, Rac, RhoGDI (loading control) and integrin β_1 (left margin) in cytoplasmic (Cyt) and membrane (M) protein fractions of 293T cells expressing recombinant Flag-tagged TIPE2 and hemagglutinin (HA)-tagged Rac, assessed before (No IP; left) or after (middle and right) immunoprecipitation (IP) with anti-Flag or the control antibody immunoglobulin G (IgG) (below blots). (**c**) Immunoblot analysis of Rac and TIPE2 (left margin) in lysates of wild-type and *Tipe2*$^{-/-}$ BMDMs (above lanes) cultured with (+) or without (–) supernatants of L929 mouse fibroblasts (L929 sup) or stimulation for 5 min with CCL2 (grid below blots), assessed before (Lysate; left) or after (middle and right) immunoprecipitation with anti-Rac or IgG (below blots). (**d**) Immunoblot analysis of TIPE2 and Rac (left margin) in lysates of dHL-60 cells, assessed before (left) or after (right) immunoprecipitation with anti-TIPE2 or IgG (above lanes). (**e**–**h**) Confocal microscopy of F-actin (**e**) and p-AKT(T308) (**f**), as well as DAPI, in wild-type and *Tipe2*$^{-/-}$ BMNs pretreated with NSC24766 and subjected to point-source stimulation with CXCL8 (**e**,**f**), and frequency of such cells (and cells not pretreated with NSC24766 (No Rac inh; above plot) with polarized or unpolarized distribution (key) of F-actin (**g**) or p-AKT(T308) (**h**). Scale bars (**e**,**f**), 5 μm. NS, not significant ($P > 0.05$); $*P < 0.05$ and $***P < 0.0001$ (Mann-Whitney *U*-test (**a**) or χ^2 test (**g**,**h**)). Data are pooled from at least two experiments with $n \geq 30$ cells per genotype (**a**; mean + s.e.m.) or from three experiments; with $n \geq 30$ cells per group, are from one experiment representative of at least three experiments (**b**–**d**) or are representative of three experiments with $n \geq 30$ cells per group (**e**,**f**).

containing both PtdIns(4,5)P_2 and PtdIns(3,4,5)P_3 but not from SUVs containing no PtdIns(3,4,5)P_3 (**Fig. 5c**). As expected, more than 81% of the TIPE2 was not bound by SUVs containing both PtdIns(4,5)P_2 and PtdIns(3,4,5)P_3, and this was significantly lower in the absence of PtdIns(3,4,5)P_3 in the SUVs (**Fig. 5d**). Thus, TIPE2 might function as a PtdIns(4,5)P_2-transfer protein only on membranes that contain PtdIns(3,4,5)P_3, a characteristic of the leading edge of cells moving by chemotaxis (**Supplementary Fig. 6d**).

TIPE2 in PtdIns(4,5)P_2 signaling and actin remodeling

Since TIPE2 was able to both bind and extract PtdIns(4,5)P_2, we investigated whether TIPE2 was able to regulate PtdIns(4,5)P_2-dependent signaling. First, we assessed the ability of TIPE2 to promote the phosphorylation of PtdIns(4,5)P_2 by active PI(3)Ks, a key process that occurs at the leading edge of migrating cells. We found that TIPE2 indeed increased the PI(3)K-catalyzed conversion of PtdIns(4,5)P_2 to PtdIns(3,4,5)P_3 up to fivefold, in a dose-dependent manner (**Fig. 6a**). 15/16Q, which strongly bound PtdIns(4,5)P_2 but had almost completely no ability to bind PtdIns(3,4,5)P_3, had a weak effect or no effect on the PI(3)K-catalyzed generation of PtdIns(3,4,5)P_3 (**Fig. 6a**). Second, we investigated if, through its interaction with PtdIns(4,5)P_2 and PtdIns(3,4,5)P_3, TIPE2 could affect actin remodeling, which is required for leading-edge formation. For this study we selected cofilin, an actin-severing protein whose activity in driving actin remodeling is inhibited by its binding to phosphoinositides[22,23]. We found that the binding of TIPE2 to SUVs containing either PtdIns(4,5)P_2 or PtdIns(3,4,5)P_3 led to a small decrease in the interaction of phosphoinositides with cofilin (**Fig. 6b**,**c**). In contrast, the interaction of cofilin with SUVs containing both PtdIns(4,5)P_2 and PtdIns(3,4,5)P_3 was reduced for more than sevenfold by TIPE2 (**Fig. 6b**,**c**). The effect of 15/16Q on the binding of cofilin to the SUVs was similar to that of wild-type TIPE2, but to a lesser degree, due presumably to its weaker binding to phosphoinositides (**Fig. 6b**,**c**). The expression of 15/16Q in dHL-60T neutrophils 'rescued' the polarization defect only partially (**Supplementary Fig. 6e**).

To understand the effect of the binding of TIPE2 to phosphoinositides on cofilin activity, we assessed cofilin-induced depolymerization of F-actin in the presence or absence of purified TIPE2 protein and phosphoinositides. SUVs containing either PtdIns(4,5)P_2 alone or PtdIns(4,5)P_2 plus PtdIns(3,4,5)P_3 significantly decreased the cofilin-induced depolymerization of F-actin (**Fig. 6d**,**e** and **Supplementary Fig. 7a**,**b**). However, TIPE2 'rescued' only the decrease in F-actin depolymerization caused by SUVs containing both PtdIns(4,5)P_2 and PtdIns(3,4,5)P_3 (**Fig. 6d**,**e** and **Supplementary Fig. 7a**,**b**). PtdIns(3,4,5)P_3, TIPE2 or control protein alone had no effect on the depolymerization of F-actin (**Fig. 6f**, **Supplementary Fig. 7c** and data not shown). These results indicated that the ability of TIPE2 to extract PtdIns(4,5)P_2 from PtdIns(3,4,5)P_3-rich membranes affected the cofilin-induced remodeling of F-actin.

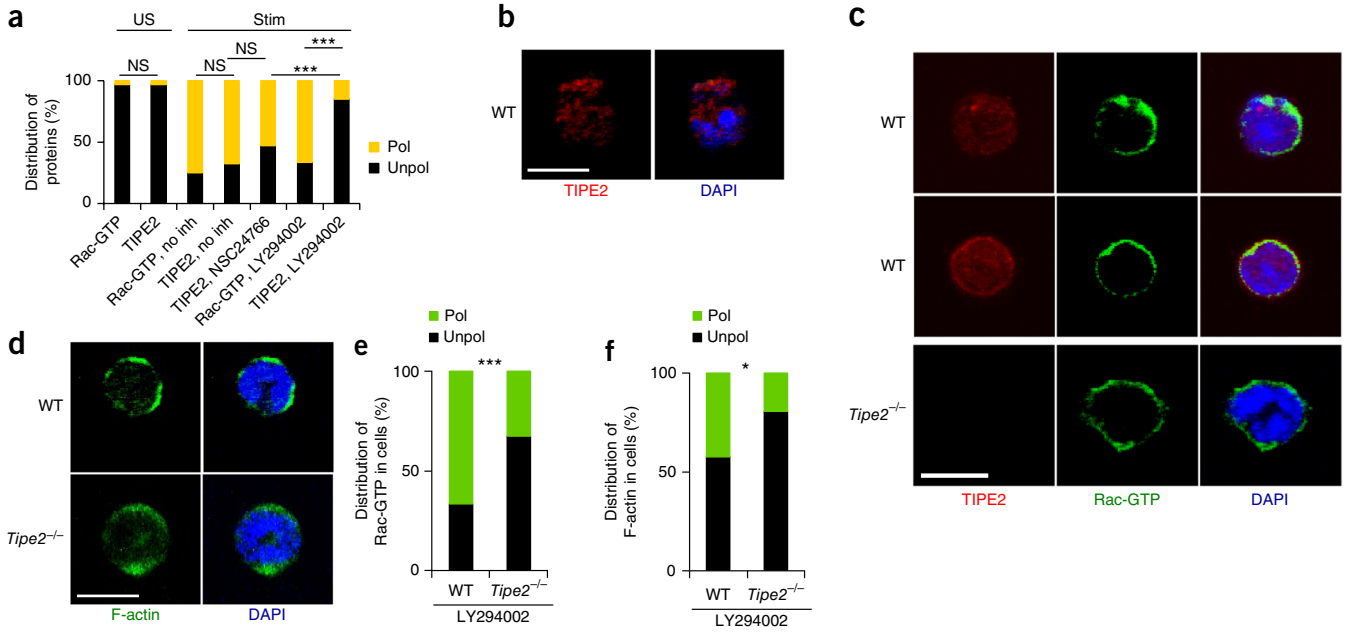

Figure 4 Rac-independent functions of TIPE2 in cells moving by chemotaxis. (**a**) Frequency of cells with polarized or unpolarized distribution (key) of various proteins (horizontal axis), among wild-type BMNs left unstimulated or subjected to point-source stimulation with CXCL8 (above plot), with or without pretreatment with the Rac inhibitor NSC24766 or PI(3)K inhibitor LY294002 (horizontal axis). (**b**–**f**) Confocal microscopy of the subcellular distribution of TIPE2 (**b**), TIPE2 and Rac-GTP (**c**) or F-actin (**d**) in wild-type and *Tipe2*$^{-/-}$ BMNs pretreated with NSC24766 (**b**) or LY294002 (**c**,**d**) and subjected to point-source stimulation with CXCL8 (**b**–**d**), and frequency of cells with polarized or unpolarized distribution (key) of Rac-GTP (**e**) or F-actin (**f**), among such cells pretreated with LY294002 and subjected to point-source stimulation with CXCL8 (**e**,**f**). Scale bars (**b**–**d**), 5 μm. $^{*}P < 0.05$ and $^{***}P < 0.001$ (χ^2 test (**a**,**e**,**f**)). Data are pooled from at three experiments with $n \geq 30$ cells per group (**a**,**e**,**f**) or are representative of at three experiments with $n \geq 30$ cells per group (**b**–**d**).

TIPE2 in neural inflammation

The directional migration of leukocytes into the central nervous system is crucial for the development of multiple sclerosis in humans and of experimental autoimmune encephalomyelitis (EAE) in mice[24,25]. Notably, *Tipe2*$^{-/-}$ mice exhibited significantly delayed onset of EAE and lower clinical scores, relative to those of wild-type mice (**Fig. 7a**). Histological analysis of spinal-cord sections from mice with EAE revealed more-severe infiltration of leukocytes in the wild-type group than in the *Tipe2*$^{-/-}$ group (**Fig. 7b**). Experiments with bone-marrow chimeras established that TIPE2 expressed by bone-marrow-derived cells contributed to the difference between wild-type mice and *Tipe2*$^{-/-}$ mice in EAE: wild-type mice that received *Tipe2*$^{-/-}$ bone-marrow cells developed significantly delayed and diminished EAE relative to that of wild-type mice that received wild-type bone-marrow cells (**Fig. 7c**). Notably, the resistance of *Tipe2*$^{-/-}$ mice to EAE was not caused by a reduction in T cell responses to myelin oligodendrocyte glycoprotein (MOG). *Tipe2*$^{-/-}$ splenocytes isolated from mice 9 d after the induction of EAE produced concentrations of the cytokines

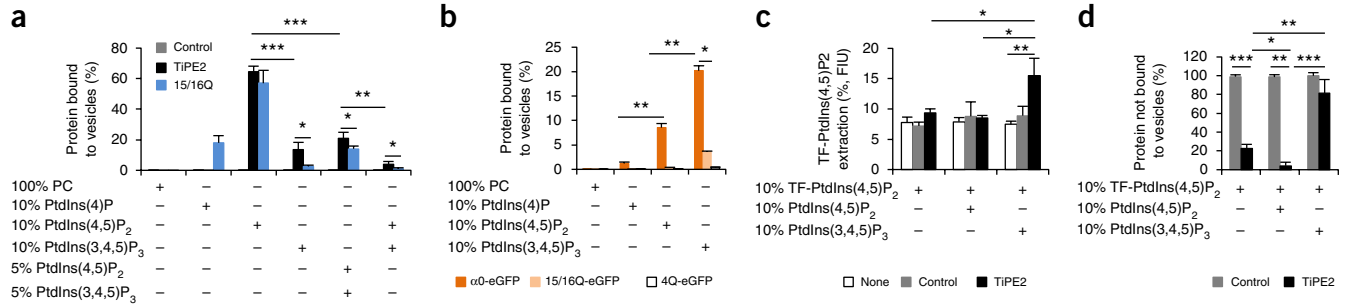

Figure 5 TIPE2 functions as a PtdIns(4,5)P_2-transfer protein in lipid bilayers enriched for PtdIns(3,4,5)P_3. (**a**,**b**) Phosphoinositide-binding assay showing the proportion of TIPE2, 15/16Q or control protein (**a**) and of eGFP-fused wild-type α0, 15/16Q or 4Q (α0 helix of TIPE2 with the lysine residues at positions 15,16, 20 plus the arginine residue at position 24 replaced with glutamines) (**b**) bound to SUVs containing 100% phosphatidylcholine (PC) or various percentages of PtdIns(4)P, PtdIns(4,5)P_2 and PtdIns(3,4,5)P_2 (grid beneath plot). (**c**) Phosphoinositide-extraction assay showing the proportion of PtdIns(4,5)P_2 (labeled with the fluorescent dye TopFluor) extracted from SUVs containing 10% TopFluor-labeled PtdIns(4,5)P_2 (TF-PtdIns(4,5)P_2) with (+) or without (–) 10% unlabeled PtdIns(4,5)P_2 and PtdIns(3,4,5)P_2 (grid beneath plot), in the presence of no added protein (None), control protein or TIPE2 (key); results are presented as fluorescence intensity units (FIU). (**d**) Phosphoinositide-extraction assay showing the proportion of control protein or TIPE2 that remained not bound to SUVs as in **c**. $^{*}P < 0.05$, $^{**}P < 0.01$ and $^{***}P < 0.001$ (unpaired Student *t*-test). Data are pooled from at least three independent experiments (mean + s.d.).

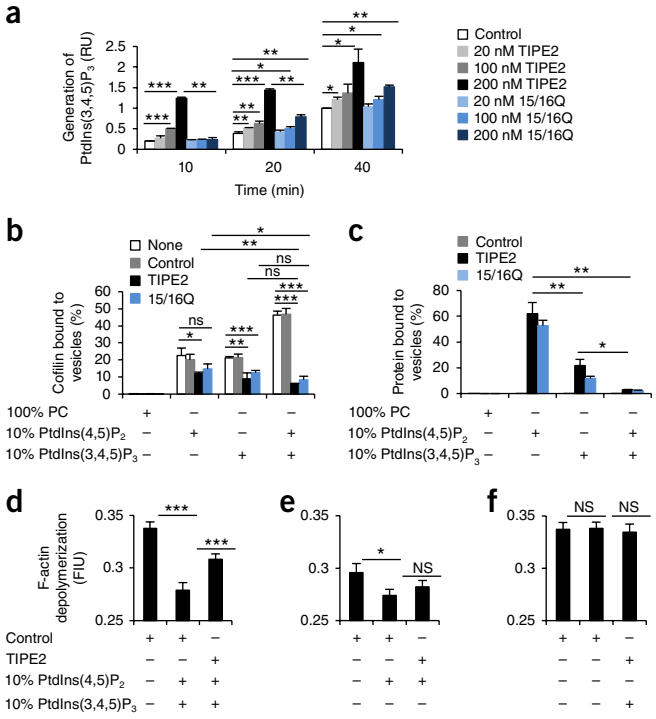

Figure 6 TIPE2 controls phosphoinositide signaling through PtdIns(3,4,5)P_3-dependent mechanisms. (**a**) PI(3)K-catalyzed generation of PtdIns(3,4,5)P_3 over time (horizontal axis) in the presence of control protein (Control) or various concentrations of TIPE2 or 15/16Q (key); results are presented relative to those obtained at 40 min with control protein, set as 1. (**b**) Phosphoinositide-binding assay showing the proportion of cofilin bound to SUVs containing 100% phosphatidylcholine or various combinations of 10% PtdIns(4,5)P_2 and PtdIns(3,4,5)P_3 (grid beneath plot), in the presence of no protein (None), control protein, TIPE2 or 15/16Q (key). (**c**) Phosphoinositide-binding assay showing the proportion of control protein, TIPE2 or 15/16Q (key) bound to SUVs as in **b** (grid beneath plot). (**d**–**f**) Cofilin-dependent depolymerization of F-actin in the presence of various combinations of control protein or TIPE2 plus SUVs containing 10% PtdIns(4,5)P_2 and/or PtdIns(3,4,5)P_3 or not (grid beneath plot). $^*P < 0.05$, $^{**}P < 0.01$ and $P < 0.001$ (unpaired Student *t*-test). Data are pooled from at least three experiments (mean + s.d. (**a**–**c**) or mean + s.e.m. (**d**–**f**)).

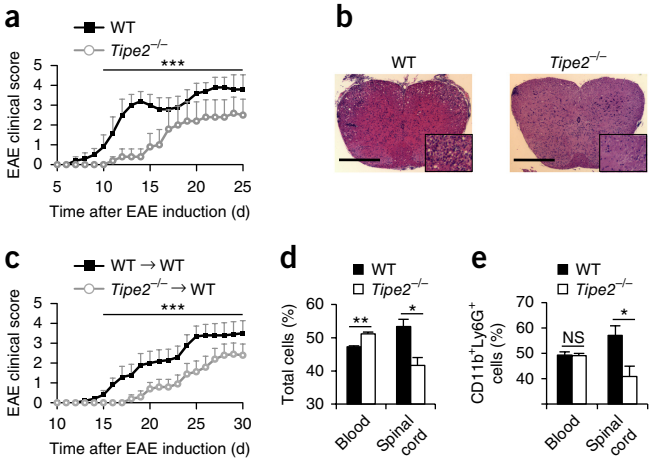

Figure 7 Diminished encephalomyelitis and infiltration of leukocytes into the nervous tissue of *Tipe2*$^{-/-}$ mice. (**a**) Daily clinical scores of *Tipe2*$^{-/-}$ and wild-type mice immunized with MOG peptide for the induction of EAE. (**b**) Microscopy of spinal-cord sections from *Tipe2*$^{-/-}$ and wild-type mice 25 d after immunization as in **a**, stained with hematoxylin and eosin; inset, enlargement (3×) of outlined area in main image. Scale bars, 500 µm. (**c**) Daily clinical scores of wild-type host mice sub-lethally irradiated and given intravenous injection (→) of *Tipe2*$^{-/-}$ or wild-type bone marrow cells (key), followed by immunization with MOG 7 weeks later for the induction of EAE. (**d**,**e**) Frequency of wild-type and *Tipe2*$^{-/-}$ (key) leukocytes (Total cells) (**d**) and CD11b$^+$Ly6G$^+$ cells (**e**) in the blood and spinal-cord leukocyte preparations (Spinal cord) of wild-type mice sub-lethally irradiated and given injection of a mixture of wild-type and *Tipe2*$^{-/-}$ bone marrow cells (at a ratio of 1:1), followed by immunization with MOG 7 weeks later for the induction of EAE, and analysis, by flow cytometry, on the day of the disease onset. $^*P < 0.05$; $^{**}P < 0.01$ and $^{***}P < 0.001$, differences after day 10 (in **a**) or day 16 (in **c**) (Mann-Whitney *U*-test (**a**,**c**) or unpaired Student *t*-test (**d**,**e**)). Data are pooled from three experiments with $n = 8$ host mice (**a**,**b**) or $n = 10$ host mice (**c**) (**a**–**c**; mean + s.e.m. in **a**,**c**) or two experiments with $n = 3$ host mice (**d**,**e**; mean + s.e.m.).

IL-2, IFN-γ and IL-17 after stimulation with MOG *in vitro* that were similar to or slightly greater than those produced by wild-type splenocytes (**Supplementary Fig. 8**). To determine whether the diminished EAE of *Tipe2*$^{-/-}$ mice was related to decreased migration of leukocytes, we generated mixed-bone-marrow chimeras with both *Tipe2*$^{-/-}$ bone-marrow-derived cells and wild-type bone-marrow-derived cells. At the onset of EAE, we observed significantly fewer total and CD11b$^+$Ly6G$^+$*Tipe2*$^{-/-}$ leukocytes than their wild-type counterparts in the spinal cord of the same mouse (**Fig. 7d**,**e**). Thus, TIPE2 had a crucial role in controlling infiltration by leukocytes during neural inflammation.

DISCUSSION

Leukocyte chemotaxis is essential for immunological defense and surveillance[26–28]. Effective elimination of pathogens and tissue repair depend on well-coordinated leukocyte chemotaxis, and its dysregulation can lead to severe infectious disease. On the other hand, directed migration of leukocytes into inflamed tissues is a common pathological process of many autoimmune diseases. Blocking leukocyte chemotaxis with the drug natalizumab or fingolimod is effective for the treatment of autoimmune diseases such as multiple sclerosis. Therefore, understanding the molecular events that regulate chemotaxis might help to identify new drug targets for the treatment of inflammatory and infectious disorders[26,28].

Several lines of evidence presented in this study established that TIPE2, a phosphoinositide-transfer protein of TIPE family, controlled leukocyte chemotaxis by acting as a polarizer, or a 'dual-role regulator' of signaling and cytoskeletal activities, in cells moving by chemotaxis. TIPE2 acts as an inhibitor of Rac, suppressing Rac-dependent polymerization of actin and activation of PI(3)Kp110β–AKT[29–31]. This action of TIPE2 promotes the formation of trailing edges and prevents the generation of secondary leading edges. TIPE2 can also function as a PtdIns(4,5)P_2-transfer protein, extracting PtdIns(4,5)P_2 from PtdIns(3,4,5)P_3-containing membranes and shuttling it in its hydrophobic cavity. This latter activity of TIPE2 is probably 'excited' by PtdIns(3,4,5)P_3 generated locally by PI(3)Kp110γ, a kinase responsible for the early-phase generation of PtdIns(3,4,5)P_3 in response to the activation of GPCRs[31–33]. By 'presenting' PtdIns(4,5)P_2 to PI(3)Ks and enhancing the generation of PtdIns(3,4,5)P_3 at PtdIns(3,4,5)P_3-containing membranes, TIPE2 reinforces a positive feedback loop that amplifies the PI(3)K signaling. PtdIns(3,4,5)P_3 in turn activates Rac guanine-nucleotide-exchange factors, which results in the activation of Rac and subsequent actin polymerization at the PtdIns(3,4,5)

P_3-rich leading edges[2]. Additionally, TIPE2 also enhances actin dynamics by extracting PtdIns(4,5)P_2 from PtdIns(3,4,5)P_3-rich membranes and sequestering it from actin-modifying proteins and thereby further promotes leading-edge formation. Published work has indicated that decreasing the abundance of PtdIns(4,5)P_2 lowers the threshold for excitability of the signaling network and promotes the formation of leading-edge protrusions[34]. It is possible that by extracting PtdIns(4,5)P_2 from PtdIns(3,4,5)P_3-rich membranes alone, TIPE2 contributes to leading-edge formation. Therefore, using a coincidence-detection strategy (i.e., active only when both PtdIns(4,5)P_2 and PtdIns(3,4,5)P_3 are present), TIPE2 enhances the GPCR signaling only at the side of the cell facing the source of chemoattractants and guides the leading-edge formation in a spatial-specific manner. These findings are consistent with the proposed models of chemotaxis on flat two-dimensional surfaces that predict the existence of both local enhancers and global inhibitors that are required for directional migration[1,4–6].

Tipe2$^{-/-}$ myeloid cells exhibited impaired chemotaxis relative to that of wild-type cells in two *in vivo* models: the acute peritonitis model and EAE. Leukocytes migrate through different tissues characterized by diverse composition and geometry to reach sites of inflammation. To acquire mechanistic information on chemotaxis, we used two-dimensional *in vitro* systems. However, these systems might not fully reflect the diversity and complexity of tissues *in vivo*[35–37]. For example, PI(3)K is much more critical for chemotaxis *in vivo* than in two-dimensional systems[38]. At the same time, the branched F-actin that is essential for chemotaxis on two-dimensional surfaces has a role only in directional selection in three-dimensional systems[35–37]. Future studies of the TIPE2-dependent effects in other models of leukocyte migration might help to further elucidate the mechanisms of chemotaxis regulation *in vivo*.

The results reported here indicated a crucial role for TIPE2 in the infiltration of leukocytes into neural tissue in EAE. Although this was probably mediated through chemotaxis, TIPE2 might also regulate EAE through additional mechanisms. For example, MOG-specific T cell responses in TIPE2-deficient mice were enhanced slightly relative to those of wild-type mice. That result is consistent with published reports showing that TIPE2 is important for preventing hyper-responsiveness of the immune system[18,19,39]. The regulation of Rac by TIPE2 is probably involved in both chemotaxis and the control of hyper-responsiveness during EAE. Thus, TIPE2 is crucial for organ-specific inflammation, and inhibition of TIPE2 might be beneficial for the treatment of inflammatory diseases such as multiple sclerosis.

METHODS

Methods, including statements of data availability and any associated accession codes and references, are available in the online version of the paper.

Note: Any Supplementary Information and Source Data files are available in the online version of the paper.

ACKNOWLEDGMENTS

We thank W. Pear (University of Pennsylvania) for NGFR vector; M. Lemmon (University of Pennsylvania) for the peGFP-GRP1-PH vector and for discussions; G. Luo, N. Li, D. Johnson, A. Stout, J. Zhao, G. Ruthel, the CDB Microscopy Core, and the PennVet Imaging Core for discussions and/or technical assistance. Supported by the US National Institutes of Health (AI121166, AI099216, and AI50059 to Y.H.C.; and T32CA009140 to A.E.B.) and the National Multiple Sclerosis Society (1501-02782 to Y.H.C.).

AUTHOR CONTRIBUTIONS

S.A.F., Z.W. and Y.H.C. conceived of the study; S.A.F. and Y.H.C. wrote the article; S.A.F. designed and performed the experiments and analyzed the data; Z.W. designed and performed the *in vivo* experiments; A.Z., A.E.B., T.P.P., W.X., M.L., T.C., J.R.G and A.V. were involved in the design or execution of several experiments; H.S. bred mice and performed μ-slide migration assay; and Y.H.C. supervised the study.

COMPETING FINANCIAL INTERESTS

The authors declare no competing financial interests.

1. Swaney, K.F., Huang, C.-H. & Devreotes, P.N. Eukaryotic chemotaxis: a network of signaling pathways controls motility, directional sensing, and polarity. *Annu. Rev. Biophys.* **39**, 265–289 (2010).
2. Merlot, S. & Firtel, R.A. Leading the way: directional sensing through phosphatidylinositol 3-kinase and other signaling pathways. *J. Cell Sci.* **116**, 3471–3478 (2003).
3. Deng, Q. & Huttenlocher, A. Leukocyte migration from a fish eye's view. *J. Cell Sci.* **125**, 3949–3956 (2012).
4. Iglesias, P.A. & Devreotes, P.N. Biased excitable networks: how cells direct motion in response to gradients. *Curr. Opin. Cell Biol.* **24**, 245–253 (2012).
5. Huang, C.-H., Tang, M., Shi, C., Iglesias, P.A. & Devreotes, P.N. An excitable signal integrator couples to an idling cytoskeletal oscillator to drive cell migration. *Nat. Cell Biol.* **15**, 1307–1316 (2013).
6. Tang, M. *et al.* Evolutionarily conserved coupling of adaptive and excitable networks mediates eukaryotic chemotaxis. *Nat. Commun.* **5**, 5175 (2014).
7. Ahn, S.-H. *et al.* Two genes on A/J chromosome 18 are associated with susceptibility to *Staphylococcus aureus* infection by combined microarray and QTL analyses. *PLoS Pathog.* **6**, e1001088 (2010).
8. Zhang, C. *et al.* Role of SCC-S2 in experimental metastasis and modulation of VEGFR-2, MMP-1, and MMP-9 expression. *Mol. Ther.* **13**, 947–955 (2006).
9. Zhang, Y. *et al.* Tumor necrosis factor-α induced protein 8 polymorphism and risk of non-Hodgkin's lymphoma in a Chinese population: a case-control study. *PLoS One* **7**, e37846 (2012).
10. Fayngerts, S.A. *et al.* TIPE3 is the transfer protein of lipid second messengers that promote cancer. *Cancer Cell* **26**, 465–478 (2014).
11. Ma, Y. *et al.* The expression and significance of TIPE2 in peripheral blood mononuclear cells from asthmatic children. *Scand. J. Immunol.* **78**, 523–528 (2013).
12. Wang, L., Song, Y. & Men, X. Variance of TNFAIP8 expression between tumor tissues and tumor-infiltrating CD4$^+$ and CD8$^+$ T cells in non-small cell lung cancer. *Tumour Biol.* **35**, 2319–2325 (2014).
13. Xi, W. *et al.* Roles of TIPE2 in hepatitis B virus-induced hepatic inflammation in humans and mice. *Mol. Immunol.* **48**, 1203–1208 (2011).
14. Yang, M. *et al.* TNFAIP8 overexpression is associated with lymph node metastasis and poor prognosis in intestinal-type gastric adenocarcinoma. *Histopathology* **65**, 517–526 (2014).
15. Zhang, C. *et al.* The significance of TNFAIP8 in prostate cancer response to radiation and docetaxel and disease recurrence. *Int. J. Cancer* **133**, 31–42 (2013).
16. Gus-Brautbar, Y. *et al.* The anti-inflammatory TIPE2 is an inhibitor of the oncogenic Ras. *Mol. Cell* **45**, 610–618 (2012).
17. Zhang, X. *et al.* Crystal structure of TIPE2 provides insights into immune homeostasis. *Nat. Struct. Mol. Biol.* **16**, 89–90 (2009).
18. Wang, Z. *et al.* TIPE2 protein serves as a negative regulator of phagocytosis and oxidative burst during infection. *Proc. Natl. Acad. Sci. USA* **109**, 15413–15418 (2012).
19. Sun, H. *et al.* TIPE2, a negative regulator of innate and adaptive immunity that maintains immune homeostasis. *Cell* **133**, 415–426 (2008).
20. Wrighton, K.H. Sensing and controlling protein dynamics. *Nat. Rev. Mol. Cell Biol.* **11**, 680–681 (2010).
21. Schaaf, G. *et al.* Functional anatomy of phospholipid binding and regulation of phosphoinositide homeostasis by proteins of the sec14 superfamily. *Mol. Cell* **29**, 191–206 (2008).
22. Ghosh, M. *et al.* Cofilin promotes actin polymerization and defines the direction of cell motility. *Science* **304**, 743–746 (2004).
23. Bravo-Cordero, J.J., Magalhaes, M.A.O., Eddy, R.J., Hodgson, L. & Condeelis, J. Functions of cofilin in cell locomotion and invasion. *Nat. Rev. Mol. Cell Biol.* **14**, 405–415 (2013).
24. Steinbach, K., Piedavent, M., Bauer, S., Neumann, J.T. & Friese, M.A. Neutrophils amplify autoimmune central nervous system infiltrates by maturing local APCs. *J. Immunol.* **191**, 4531–4539 (2013).
25. Steinman, L. Multiple sclerosis: a two-stage disease. *Nat. Immunol.* **2**, 762–764 (2001).
26. Luster, A.D., Alon, R. & von Andrian, U.H. Immune cell migration in inflammation: present and future therapeutic targets. *Nat. Immunol.* **6**, 1182–1190 (2005).
27. Friedl, P. & Weigelin, B. Interstitial leukocyte migration and immune function. *Nat. Immunol.* **9**, 960–969 (2008).
28. de Oliveira, S., Rosowski, E.E. & Huttenlocher, A. Neutrophil migration in infection and wound repair: going forward in reverse. *Nat. Rev. Immunol.* **16**, 378–391 (2016).
29. Fritsch, R. *et al.* RAS and RHO families of GTPases directly regulate distinct phosphoinositide 3-kinase isoforms. *Cell* **153**, 1050–1063 (2013).

30. Sadhu, C., Masinovsky, B., Dick, K., Sowell, C.G. & Staunton, D.E. Essential role of phosphoinositide 3-kinase delta in neutrophil directional movement. *J. Immunol.* **170**, 2647–2654 (2003).
31. Boulven, I. *et al*. Class IA phosphatidylinositide 3-kinases, rather than p110 gamma, regulate formyl-methionyl-leucyl-phenylalanine-stimulated chemotaxis and superoxide production in differentiated neutrophil-like PLB-985 cells. *J. Immunol.* **176**, 7621–7627 (2006).
32. Ferguson, G.J. *et al*. PI(3)Kγ has an important context-dependent role in neutrophil chemokinesis. *Nat. Cell Biol.* **9**, 86–91 (2007).
33. Tang, W. *et al*. A PLCβ/PI3Kγ-GSK3 signaling pathway regulates cofilin phosphatase slingshot2 and neutrophil polarization and chemotaxis. *Dev. Cell* **21**, 1038–1050 (2011).
34. Miao, Y. *et al*. Altering the threshold of an excitable signal transduction network changes cell migratory modes. *Nat. Cell Biol.* **19**, 329–340 (2017).
35. Wilson, K. *et al*. Mechanisms of leading edge protrusion in interstitial migration. *Nat. Commun.* **4**, 2896 (2013).
36. Vargas, P. *et al*. Innate control of actin nucleation determines two distinct migration behaviours in dendritic cells. *Nat. Cell Biol.* **18**, 43–53 (2016).
37. Leithner, A. *et al*. Diversified actin protrusions promote environmental exploration but are dispensable for locomotion of leukocytes. *Nat. Cell Biol.* **18**, 1253–1259 (2016).
38. Yoo, S.K. *et al*. Differential regulation of protrusion and polarity by PI3K during neutrophil motility in live zebrafish. *Dev. Cell* **18**, 226–236 (2010).
39. Sun, H. *et al*. TIPE2 controls innate immunity to RNA by targeting the phosphatidylinositol 3-kinase-Rac pathway. *J. Immunol.* **189**, 2768–2773 (2012).

ONLINE METHODS

Mice. *Tipe2*$^{-/-}$ C57BL/6 mice were generated as described[18,19]. Wild-type C57BL/6 mice expressing CD45.1 or CD45.2 were purchased from Jackson Laboratories. Mice were housed in the University of Pennsylvania Animal Care Facilities under pathogen-free conditions. All animal procedures were preapproved by the Institutional Animal Care and Use Committee of the University of Pennsylvania, and all experiments conform to the relevant regulatory standards.

The acute peritonitis model for studying myeloid-cell migration *in vivo*. 6-week-old wild-type CD45.1$^+$ mice (recipient mice) were given intraperitoneal injection of Freund's adjuvant (0.5 ml/mouse) to induce acute peritonitis. 24 h later, they were given intravenous injection of carboxyfluorescein succinimidyl ester (CFSE)-labeled bone marrow cells (1×10^7 per mouse) from 6-week-old *Tipe2*$^{-/-}$ CD45.2$^+$ and wild-type CD45.1$^+$ mice, mixed at 1:1 ratio. Recipient mice were killed 16 h later and their peritoneal cells were collected. The peritoneal cells were stained with anti-CD45.1-PE (eBioscience), anti-CD45.2-PerCP/Cy5.5 (eBioscience) and anti-Ly6G-APC (eBioscience), and the frequency of *Tipe2*$^{-/-}$CD45.2$^+$CFSE$^+$Ly6G$^+$ and wild-type CD45.1$^+$CFSE$^+$Ly6G$^+$ cells was determined by flow cytometry. The number of mice required for the experiment was calculated using Power and Sample Size Calculation (PS) software (Vanderbilt University). The paired Student *t*-test was used to assess the statistical significance of the results.

Experimental autoimmune encephalomyelitis (EAE). The induction and assignment of clinical scores for EAE in wild-type and *Tipe2*$^{-/-}$ mice were performed as described previously[40,41]. Myelin oligodendrocyte glycoprotein (MOG) peptide (amino acids 35–55) was used as the autoantigen. Spinal cords of mice were harvested at the end of each experiment, then were fixed, paraffin-embedded and sectioned. The sections were stained with hematoxylin and eosin and were analyzed using a wide field light microscope. To determine the contribution of TIPE2 expressed by bone marrow-derived cells in EAE, a bone-marrow–chimera approach was used[42]. In brief, wild-type mice were sub-lethally irradiated and given intravenous injection of bone marrow cells from *Tipe2*$^{-/-}$ or wild-type mice (1.5×10^7 cells per mouse). 7 weeks later, EAE was induced and examined as described[40,41]. The number of mice used for the experiments was calculated using PS software. Mann-Whitley *U* test was used to assess the statistical significance of the results.

To study the migration of wild-type and *Tipe2*$^{-/-}$ leukocytes in mice with EAE, a mixed–bone-marrow chimera approach was used[42]. In brief, 6-week-old wild-type CD45.1$^+$ mice (recipient mice) were sub-lethally irradiated and given intravenous injection of bone marrow cells from 6-week-old *Tipe2*$^{-/-}$ CD45.2$^+$ and wild-type CD45.1$^+$ mice, mixed at 1:1 ratio (1.5×10^7 cells per mouse). 7 weeks later, the recipient mice were immunized with MOG to induce EAE and were killed on the day of the disease onset (with a EAE clinical score of 1). Blood and spinal cords of recipient mice (collected after perfusion of recipient mice with 30 ml PBS via the heart) were used for the isolation of leukocytes by centrifugation through a Percoll gradient. The leukocytes were stained with anti-CD45.1-PE (A20) (eBioscience 12-0453-82), CD45.2-PerCP/Cy5.5 (104) (eBioscience 45-0454-82), anti-CD45.1-PE (A20) (eBioscience 12-0453-82), anti-CD45.2-PerCP/Cy5.5 (104) (eBioscience 45-0454-82), anti-Ly6G-APC (RB6-8C5) (eBioscience 17-5931-82) and anti-CD11b-FITC (M1/70) (eBioscience 11-0112-82), and the frequency of total *Tipe2*$^{-/-}$ CD45.2$^+$ and wild-type CD45.1$^+$ leukocytes or *Tipe2*$^{-/-}$ CD45.2$^+$CFSE$^+$Ly6G$^+$ and wild-type CD45.1$^+$CFSE$^+$Ly6G cells, respectively, among total leukocytes was determined by flow cytometry. The number of mice ($n = 3$) required for the experiments was estimated using PS software (Vanderbilt University). Student's *t*-test was used to assess the statistical significance of the results.

Generation of BMDMs, plasmid DNA transfection, retrovirus preparation and infection, immunoblot analysis, co-immunoprecipitation, and ELISA. Assays were performed as previously described[10,18,43]. The purity of BMDM populations was greater than 95%, as determined by flow cytometry after staining of cells with anti-CD11b-FITC (M1/70) (eBioscience 11-0112-82) and anti-F4/80-APC (BM8) (eBioscience 11-4801-82), and the viability was greater than 99%, as determined by trypan blue staining. Antibodies to the following antigens were used for immunoblot analysis and co-immunoprecipitation: Rac1 (23A8) (EMD Millipore 05-389), Rac1/2/3 (Cell Signaling Technology 2465), RhoGDI (Cell Signaling Technology 2564), AKT (Cell Signaling Technology 9272), Aktphosphorylated at Thr308 (L32A4) (Cell Signaling Technology 5106), Aktphosphorylated at Ser473 (587F11) (Cell Signaling Technology 4051), GSK-3β phosphorylated at Ser9 (Cell Signaling Technology 9336), cofilin (D3F9) (Cell Signaling Technology 5175), cofilin phosphorylated at Ser3 (77G2) (Cell Signaling Technology 3313), PAK1 phosphorylated at Ser144 and PAK2 phosphorylated atSer141 (Cell Signaling Technology 2606), LIMK1 phosphorylated at Thr508 and LIMK2 phosphorylated atThr505 (Cell Signaling Technology 3841), p44/42 MAPK (Erk1/2) (Cell Signaling Technology 9102), p44/42 MAPK (Erk1/2) phosphorylated at Thr202 and Tyr204) (Cell Signaling Technology 9101), p38 MAPK phosphorylated at Thr180 and Tyr182 (D3F9) (Cell Signaling Technology 4511), mTOR (Cell Signaling Technology 2972), GAPDH (D16H11) (Cell Signaling Technology 5174), integrin β1(Cell Signaling Technology 4706), TIPE2 (Proteintech 15940-1-AP), Flag (M2) (Sigma-Aldrich F1804), Actin (AC15) (Sigma-Aldrich A1978), HA-Tag (6E2) (Cell Signaling Technology 2999) and control IgG (Santa Cruz Biotechnology sc-2027). Rabbit IgG, HRP-linked whole antibody (GE Healthcare Life Sciences NA934) and mouse IgG, HRP-linked whole antibody (GE Healthcare Life Sciences NA931) were also used.

Isolation of BMNs and blood neutrophils (BNs). Mouse blood was drawn from retro-orbital plexus of the eyes, and bone marrow was collected from femur and tibia bones. BNs and BMNs were isolated using Histopaque-1119 and Histopaque-1077 (Sigma-Aldrich) according to the manufacturer's instructions. The purity of BNs and BMNs populations was greater than 90%, as determined by flow cytometry after staining with anti-Ly6G-APC (RB6-8C5) (eBioscience 17-5931-82), and the viability was greater than 99%, as determined by trypan blue staining.

Generation of TIPE2-deficient HL-60 cells (HL-60T) and HL-60T cells expressing TIPE2 or 15/16Q. HL-60 cells were obtained from ATCC and were cultured in RPMI-1640 medium supplemented with 15% FBS. TIPE2-deficient HL-60 cells (HL-60T) and control HL-60 cells (HL-60C) were generated using the CRISPR-Cas9 system and TIPE2-specific single-guide RNA (sgTIPE2) or non-targeting control single-guide RNA (sgControl) as described[44]. To generate HL-60T cells expressing TIPE2 (TIPE2-HL-60T) or 15/16Q, HL-60T cells were infected with retrovirus carrying cDNA encoding either TIPE2 or 15/16Q and cDNA encoding nerve growth factor receptor (NGFR). Control HL-60C cells were infected with retrovirus carrying cDNA encoding NGFR alone (NGFR vector is a gift from W. Pear, University of Pennsylvania). NGFR$^+$ cells were isolated by flow cytometry. Before being used in the assays, HL-60 cells were treated with 1.25% DMSO and 25 ng/ml G-CSF for 5 d to generate differentiated HL-60 neutrophils (dHL-60 cells)[45].

Transwell migration assay. For BMDMs, cells were allowed to 'rest' in DMEM for 1 h. For BMNs, cells were allowed to 'rest' in Hanks' balanced salt solution (HBSS) containing 0.1% BSA (fatty acid free) for 1 h. For dHL-60C cells, dHL-60T cells and TIPE2-expressing dHL-60T cells, the cells were stained with Calcein-AM (BD Biosciences) and were allowed to 'rest' in HBSS containing 0.1% BSA for 30 min. After the resting period, migration assays were performed using Transwells with 5.0-μm-pore filters (for BMDMs and BMNs) or 3.0-μm-pore filters (for dHL-60), which were coated with fibronectin (Corning)[46]. For BMDMs, CCL2 was added to the bottom well at a concentration of 10, 20 or 40 ng/ml. For BMNs, CXCL2 was added at a concentration of 10 or 50 ng/ml. For dHL-60 cells, CXCL8 was added at a concentration of 25 ng/ml. Cells were allowed to migrate for 0.5–3 h, and those migrated into the lower chamber were counted. The chemotaxis index was calculated as follows: the number of cells that migrated in response to chemoattractant / the number of cells that migrated randomly (in the absence of chemoattractants). Student's *t*-test was used to assess the statistical significance of the results.

μ-slide migration assay. Wild-type and *Tipe2*$^{-/-}$ BNs were resuspended in RPMI medium supplemented with 2% FBS and were allowed to 'rest' for 30 min and then were loaded into μ–slides (Ibidi) following the manufacturer's instructions. CXCL1 was added to only one reservoir of the μ-slide at a

concentration of 200 ng/ml. Cells were recorded every 45 s for at least 2 h using a Leica DMI4000 microscope with Yokogawa CSU-X1 spinning disk confocal attachment at 10× magnification. Images were analyzed by Volocity software (Perkin Elmer) using the automated tracking protocol. Objects less than 16 μm^3 in size were excluded, and tracks were generated with the shortest-path model. A maximum distance between objects was set as 25 µm, on the basis of observed optimal tracking in the wild-type cells. Tracks of less than 200 µm were excluded. Cell velocity and vector angle between each track's starting and end points were obtained from Volocity using these settings. Velocity was defined as a cell's centroid movement (in µm/min) along the total path. Cell directionality, or the directional movement index (DMI), was defined as the cosine of the vector angle formed by the line between the cell's start point and the source of the chemoattractant, and the line between the cell's start point and the end point. A value of 1 indicates migration directly toward the chemoattractant, while a value of -1 indicates migration away from the chemoattractant. To generate representative center-zeroed tracks of individual wild-type and *Tipe2*$^{-/-}$ cells, a subset of all the tracks used in the analysis was displayed to avoid oversaturation of the image. The tracks were sorted by migration length, and the tracks with the 40 longest migration lengths are presented for each genetic background. Tracks with lengths greater than 400 µm were excluded, and tracks were selected only from the middle of the videos (track time, 25–80 min). None of these exclusions were made for the quantitative analyses. The results of a representative experiment are presented. The statistical significance of the results was evaluated by Mann-Whitney *U* test (directionality) and Student's *t*-test (velocity).

Time-lapse confocal microscopy of live neutrophils. The polarization of PtdIns(3,4,5)P_3 in migrating cells was visualized by the eGFP-tagged GRP1-PH domain, which specifically binds PtdIns(3,4,5)P_3. In brief, dHL-60C and dHL-60T neutrophils were transfected with peGFP-GRP1-PH vector (provided by M. Lemmon, University of Pennsylvania) using Amaxa cell line nucleofector kit V (Lonza) and Amaxa nucleofector II (program Y-001, Lonza). Cells were plated onto fibronectin-coated glass bottom dishes 24 h after transfection. The adherent dHL-60C and dHL-60T cells were subjected to point-source stimulation with 125 ng/ml CXCL8 at 37 °C. The migration of dHL-60C and dHL-60T neutrophils along the CXCL8 gradient was recorded every 10 s for at least 400 s using an Olympus IX71 inverted fluorescent microscope with spinning-disk confocal attachment at 60× magnification. The images were analyzed using ImageJ software. The experiment was repeated two times. More than 45 cells of each genotype were analyzed. Cell polarization was determined on the basis of the line-fluorescence-intensity profile of cells. Cells were considered polarized if the average fluorescence signal on one side of the cell was more than 1.5 times stronger than the signal on the opposite side. Results are presented as the degree of CXCL8-induced polarization of PtdIns(3,4,5)P_3, which is the difference in the frequency of polarized cells before and after stimulation with CXCL8. The statistical significance of results was evaluated by the Mann-Whitney *U*-test.

Immunofluorescence analysis and confocal microscopy of fixed neutrophils. BMNs, dHL-60C cells, dHL-60T cells and TIPE2-expressing or 15/16Q-expressing dHL-60T cells were allowed to 'rest' for 1 h in HBSS containing 0.1% BSA. Then cells were subjected to point-source stimulation with CXCL2 or CXCL8 at 1 µg/ml for 2.5 min at 37 °C (ref. 33). In several experiments, before stimulation with chemoattractants, BMNs and dHL-60 were pretreated with vehicle, Rac inhibitor (NSC24766, 200 µM, Tocris) or PI(3)K inhibitor (LY29004, 25 µM, Cell Signaling Technology) for 30 min. After stimulation, cells were fixed with 3% paraformaldehyde in phosphate-buffered saline (PBS) for 15 min at 37 °C, then were permeabilized in PBS containing 0.1% Triton X-100 and 3% BSA for 10 min at 25 °C and were blocked with PBS containing 5% normal goat serum and 3% BSA for 1 h at 25 °C. BMNs and dHL-60 cells were stained overnight at 4 °C with Phalloidin-AlexaFluor 555 (Cell Signaling Technology) in 3% BSA. Alternatively, they were first incubated overnight at 4 °C with antibody to Akt phosphorylated at Thr308 (L32A4) (Cell Signaling Technology 5106), TIPE2 (Proteintech 15940-1-AP) or Rac-GTP (NewEast Biosciences 26903) in 3% BSA, then were incubated for 1 h at 25 °C with F(ab′)$_2$ goat anti-rabbit IgG (H+L) cross-adsorbed secondary antibody Alexa Fluor 555 (ThermoFisher Scientific A-21430) and F(ab′)$_2$ goat anti-Mouse IgG/IgM (H+L) secondary antibody Alexa Fluor 488 (ThermoFisher Scientific A-10684) in 3% BSA. Isotype-matched immunoglobulins, PI(3)K-inhibitor-treated cells and Rac-inhibitor-treated cells were used as staining controls. Slides were dried and covered with ProLong Gold with DAPI (Invitrogen). Images were acquired on a Zeiss LSM 510 NLO/META and a Zeiss LSM 710 confocal microscope and were analyzed using LSM Image Browser, Zen lite (Zeiss), and ImageJ software. All images presented here are representative of at least two independent experiments. 30–120 cells of each type and condition were analyzed. Cell polarization was evaluated as described above. Results are presented as the frequency of cells of each genotype with polarized or unpolarized distribution. The statistical significance of the results was evaluated by the χ^2 test. For F-actin polarization, results are also presented as the degree of chemoattractant-induced polarization of F-actin, which is the difference in the frequency of polarized cells before and after stimulation with chemoattractant. Student's *t*-test was used to assess the statistical significance of these results. To study the spreading of wild-type and *Tipe2*$^{-/-}$ BMNs, more than 30 cells of each type and condition were measured. The spreading value of the resting wild-type BMNs was set as 1. The statistical significance of results was evaluated by the Mann-Whitney *U* test.

Adhesion assay of BMDMs and dHL-60 cells. For wild-type and *Tipe2*$^{-/-}$ BMDMs, cells were cultured overnight in DMEM supplemented with 10% FBS, were collected with 5 mM EDTA in DPBS and were allowed to 'rest' in DMEM for 1 h. Adhesion to fibronectin-coated plates of 'rested' or 'rested' and stimulated cells (with 20 ng/ml of CCL2) was assessed by staining of adherent cells with crystal violet and measurement of absorbance at 570 nm. The adhesion value of wild-type BMDMs at 15 min was set as 1. For dHL-60C cells, dHL-60T cells and TIPE2-expressing dHL-60T cells, the cells were labeled with 0.5 µM calcein-acetoxymethyl ester (Molecular Probes) for 30 min at 37 °C and were pretreated with vehicle, Rac inhibitor or PI(3)K inhibitor for 2 h at 37 °C. Then, cells were added to plates coated with fibronectin and were incubated for 5 min at 37 °C. The quantity of dHL-60 cells, dHL-60T cells and TIPE2-expressing dHL-60T cells that adhered to fibronectin was determined in a fluorescence multi-well plate reader (Molecular Devices). The adhesion value of dHL-60C cells pretreated with vehicle was set as 1. Student's *t*-test was used to assess the statistical significance of the results at each time point.

Flow-cytometry analysis of F-actin and p-AKT(T308) cellular content. Wild-type and *Tipe2*$^{-/-}$ mouse BMNs or dHL-60T cells and TIPE2-expressing dHL-60T cells were allowed to 'rest' in HBSS containing 0.1% BSA. Cells were treated with fMLP (10 µM) or CXCL2 (100 ng/ml) for 30, 60, 120 and 300 s, or not. Cells were then fixed in PBS containing 4% paraformaldehyde overnight at 4 C° and were permeabilized in PBS containing 0.1% Triton X-100 for 5 min at 25 °C. Cells were stained with rabbit antibody to Akt phosphorylated at Thr308 (L32A4) (Cell Signaling Technology 5106) or control IgG (Santa Cruz Biotechnology sc-2025) for 1 h at 25 °C, and with F(ab′)2 goat anti-rabbit IgG (H+L) cross-adsorbed secondary antibody Alexa Fluor 488 (ThermoFisher Scientific A-11070). Alexa Fluor 555 Phalloidin (Cell Signaling Technology 8953) and anti-Ly6G-APC (RB6-8C5) (eBioscience 17-5931-82) for 1 h at 25 °C, and analyzed by flow cytometry. Student's *t*-test was used to assess the statistical significance of the results at each time point.

Phosphoinositide binding and extraction assays. Recombinant His_6-TIPE2 15/16Q protein was generated by replacement of lysine at positions 15 and 16 with glutamine in wild-type His_6-TIPE2 protein. Recombinant His_6-α0-eGFP, His_6-α0 15/16Q-eGFP and His_6-α0 4Q-eGFP proteins were generated by fusion of enhanced green fluorescent protein (eGFP) with wild-type TIPE2 α0 helix or mutant TIPE2 α0 helix in which lysine at posistions 15 and 16 were replaced with glutamine (15/16Q) or lysine at positions 15,16 and 20 plus arginine at position 24 were replaced with glutamine (4Q). His_6-TIPE2 (TIPE2), His_6-TIPE2 15/16Q (15/16Q), His_6-α0-eGFP (α0-eGFP), His_6-α0 15/16Q-eGFP (α0 15/16Q-eGFP), His_6-α0 4Q-eGFP (α0 4Q-eGFP) and His_6-cofilin (cofilin) were expressed in *Escherichia coli* BL21(DE3) cells (Stratagene), were purified using Ni-charged MagBeads (GenScript) and were dialyzed using Amicon Centrifugal Filters. Purified trypsin inhibitor of *Glycine max* was used as a control protein (Sigma-Aldrich). The small unilamellar vesicles (SUVs) were produced, and sedimentation-based phosphoinositide

doi:10.1038/ni.3866

binding and extraction assays were performed as previously described[10]. In the sedimentation-based phosphoinositide-binding assay, TIPE2, 15/16Q, control protein (trypsin inhibitor), α0-eGFP, α0 15/16Q-eGFP and α0 4Q-eGFP were used at a concentration of 10 μM, and SUVs were used at a concentration of 1 mM (0.5 mM total available lipid). In the sedimentation-based phosphoinositide-binding assay of cofilin, 1 mM SUV (0.5 mM total available lipid) was pretreated with 5 μM TIPE2, 15/16Q, control protein or buffer alone for 1 h, then 5 μM cofilin was added to each reaction. After 20 min of incubation, samples were subjected to ultracentrifugation[47]. In sedimentation-based PtdIns(4,5)P_2-extraction assays, TIPE2 and control protein were used at a concentration of 10 μM, and SUVs containing fluorescence-labeled PtdIns(4,5)P_2 (TopFluor (TF)-PtdIns(4,5)P_2) were used at a concentration of 0.2 mM vesicles (0.1 mM total available lipid). Student's *t*-test was used to assess the statistical significance of the results.

PI(3)K enzymatic assay. PI(3)K enzymatic assays were performed as previously described[10,48] with minor modifications; i.e., PI(3)K was assayed at a concentration of 4 μg/ml, and SUVs were used at a concentration of 125 μM. PI(3)K-catalyzed generation of PtdIns(3,4,5)P_3 determined at 40 min in the absence of TIPE2 or 15/16Q was set as 1. Student's *t*-test was used to assess the statistical significance of the results.

F-actin-depolymerization assay. An Actin Polymerization Biochem kit (Cytoskeleton) was used to investigate the depolymerization of F-actin by cofilin in the presence or absence of TIPE2, the control protein BSA and SUVs containing 10% PtdIns(4,5)P_2, 10% PtdIns(3,4,5)P_3 or 10% PtdIns(4,5)P_2 plus 10% PtdIns(3,4,5)P_3, according to the manufacturer's instructions with minor modifications. 2 mM SUV (1 mM total available lipid) was pretreated with 11 μM TIPE2 or control protein for 1 h, then cofilin (11 μM) was added to each reaction, followed by incubation for 20 min. Additionally, cofilin (11 μM) was also incubated with TIPE2 (11 μM) or control protein (11 μM) for 20 min (control reaction). Pyrene-labeled F-actin stock was diluted with General Actin Buffer (25 mM Tris-HCl, pH 8.0, and 0.2 mM $CaCl_2$) to a concentration of 0.1 mg/ml. For each sample, 100 μl of diluted pyrene-labeled F-actin stock was used. The fluorescence was measured using an infinite 200 Pro fluorescence plate reader (Tecan) immediately before and after the addition of 10 μl of one of the following reagents: control protein (22 μM); cofilin (11 μM) plus control protein (11 μM); cofilin (11 μM) plus TIPE2 (11 μM); cofilin (11 μM) plus control protein (11 μM) plus SUVs; cofilin (11 μM) plus TIPE2 (11 μM) plus SUVs; or vehicle (25 mM HEPES and 150 mM NaCl, pH 7.5). The experiments were performed in duplicate or triplicate (technical replicates) and were repeated at least four times. The results of a representative experiment are presented. The fluorescence measurement of each sample before the addition of the reagents noted above was set as 100%. The results were fitted to one-phase exponential decay equations using GraphPad Prism to assess the degree (or span) of F-actin depolymerization for each sample, which was calculated as the difference in fluorescence before and after the addition of the reagents noted. Student's *t*-test was used to assess the statistical significance of the results. Additionally, results are also presented as the difference in the remaining F-actin over a period of time. TIPE2, control protein and SUVs alone did not affect F-actin depolymerization (data not shown).

Data availability. The data that support the findings of this study are available from the corresponding author upon request.

A **Life Sciences Reporting Summary** for this paper is available.

40. Sun, J., Hilliard, B., Xu, L. & Chen, Y.H. Essential roles of the Fas-associated death domain in autoimmune encephalomyelitis. *J. Immunol.* **175**, 4783–4788 (2005).
41. Xu, L. *et al.* Arginase and autoimmune inflammation in the central nervous system. *Immunology* **110**, 141–148 (2003).
42. Ruan, Q. *et al.* Development of Foxp3(+) regulatory t cells is driven by the c-Rel enhanceosome. *Immunity* **31**, 932–940 (2009).
43. Ruan, Q. *et al.* The Th17 immune response is controlled by the Rel-RORγ-RORγ T transcriptional axis. *J. Exp. Med.* **208**, 2321–2333 (2011).
44. Wang, T., Wei, J.J., Sabatini, D.M. & Lander, E.S. Genetic screens in human cells using the CRISPR-Cas9 system. *Science* **343**, 80–84 (2014).
45. Hirayama, A., Adachi, R., Otani, S., Kasahara, T. & Suzuki, K. Cofilin plays a critical role in IL-8-dependent chemotaxis of neutrophilic HL-60 cells through changes in phosphorylation. *J. Leukoc. Biol.* **81**, 720–728 (2007).
46. JoVE Science Education Database. The Transwell Migration Assay. *Cell Biology.* JoVE, Cambridge, MA, (2017).
47. Zhao, H., Hakala, M. & Lappalainen, P. ADF/cofilin binds phosphoinositides in a multivalent manner to act as a PIP(2)-density sensor. *Biophys. J.* **98**, 2327–2336 (2010).
48. Knight, Z.A., Feldman, M.E., Balla, A., Balla, T. & Shokat, K.M. A membrane capture assay for lipid kinase activity. *Nat. Protoc.* **2**, 2459–2466 (2007).

nature research

Corresponding author(s): Youhai H. Chen

☐ Initial submission ☐ Revised version ☒ Final submission

Life Sciences Reporting Summary

Nature Research wishes to improve the reproducibility of the work that we publish. This form is intended for publication with all accepted life science papers and provides structure for consistency and transparency in reporting. Every life science submission will use this form; some list items might not apply to an individual manuscript, but all fields must be completed for clarity.

For further information on the points included in this form, see Reporting Life Sciences Research. For further information on Nature Research policies, including our data availability policy, see Authors & Referees and the Editorial Policy Checklist.

Experimental design

1. Sample size

Describe how sample size was determined.

Sample size was calculated using the Power and Sample Size Calculation (PS) software (Vanderbilt University).

2. Data exclusions

Describe any data exclusions.

For animal studies, only 6-8 week-old wild-type and Tipe2-/- mice were utilized for experiments. It was previously shown that old Tipe2-/- mice (older that 1 year) have a high risk to develop splenomegaly. We excluded WT and Tipe2-/- mice older than 10 weeks from this study.

3. Replication

Describe whether the experimental findings were reliably reproduced.

All experimental findings were reliably reproduced.

4. Randomization

Describe how samples/organisms/participants were allocated into experimental groups.

Mice and cell samples were randomly divided into individual groups for this study.

5. Blinding

Describe whether the investigators were blinded to group allocation during data collection and/or analysis.

Researchers were not blinded about murine and cellular genotypes.

Note: all studies involving animals and/or human research participants must disclose whether blinding and randomization were used.

6. Statistical parameters

For all figures and tables that use statistical methods, confirm that the following items are present in relevant figure legends (or in the Methods section if additional space is needed).

n/a	Confirmed	
☐	☒	The exact sample size (*n*) for each experimental group/condition, given as a discrete number and unit of measurement (animals, litters, cultures, etc.)
☐	☒	A description of how samples were collected, noting whether measurements were taken from distinct samples or whether the same sample was measured repeatedly
☐	☒	A statement indicating how many times each experiment was replicated
☐	☒	The statistical test(s) used and whether they are one- or two-sided (note: only common tests should be described solely by name; more complex techniques should be described in the Methods section)
☐	☒	A description of any assumptions or corrections, such as an adjustment for multiple comparisons
☐	☒	The test results (e.g. *P* values) given as exact values whenever possible and with confidence intervals noted
☐	☒	A clear description of statistics including central tendency (e.g. median, mean) and variation (e.g. standard deviation, interquartile range)
☐	☒	Clearly defined error bars

See the web collection on statistics for biologists for further resources and guidance.

Nature Immunology: doi:10.1038/ni.3866

Software

Policy information about availability of computer code

7. Software

Describe the software used to analyze the data in this study.	Prism, excel

For manuscripts utilizing custom algorithms or software that are central to the paper but not yet described in the published literature, software must be made available to editors and reviewers upon request. We strongly encourage code deposition in a community repository (e.g. GitHub). *Nature Methods* guidance for providing algorithms and software for publication provides further information on this topic.

Materials and reagents

Policy information about availability of materials

8. Materials availability

Indicate whether there are restrictions on availability of unique materials or if these materials are only available for distribution by a for-profit company.	there aren't any restrictions

9. Antibodies

Describe the antibodies used and how they were validated for use in the system under study (i.e. assay and species).	Antibodies used for immunofluorescence analysis: anti-pAKT(T308) (Cell Signaling Technology), anti-TIPE2 (Proteintech), or anti-Rac-GTP (NewEast Biosciences, monoclonal, 26903), anti-rabbit IgG Fab-AlexaFluor 555 and anti-mouse IgM Fab-Alexa Fluor 488 (ThermoFisher Scientific). Antibodies used for Immunoprecipitation and Western blotting: anti-Rac1/2/3, RhoGDI, AKT, p-AKT (T308), p-AKT (S473), p-GSK-3β (S9), cofilin, p-cofilin (S3), p-PAK1/2 (S144/S141), p-LIMK1 (Thr508)/LIMK2 (Thr505), ERK1/2, p-ERK1/2 (T202/Y204), p-p38 (T180/Y182), mTOR, GAPDH, integrin-β1 (Cell Signaling Technology), anti-TIPE2 (Proteintech), anti-Rac1 (EMD Millipore, monoclonal, clone 23A8), anti-Flag (Sigma-Aldrich, monoclonal, M2), anti-actin (Sigma-Aldrich, monoclonal, AC-15), anti-HA (Cell Signaling Technology, monoclonal, C29F4), control IgG (Santa Cruz biotechnology), anti-rabbit IgG-HRP and anti-mouse IgG-HRP (GE Healthcare Life Sciences). Antibodies used for Flow cytometric analysis: anti-CD45.1-PE, CD45.2-PerCP/Cy5.5, Ly6G-APC and anti- CD11b-FITC, anti-F4/80-APC (eBioscience), control IgG (Santa Cruz biotechnology), anti-pAKT(T308) (Cell Signaling Technology), anti-rabbit IgG Fab-AlexaFluor 488 (ThermoFisher Scientific). Antibody were validated by using appropriate positive and negative controls.

10. Eukaryotic cell lines

a. State the source of each eukaryotic cell line used.	HL-60 (ATCC, CCL-240) 293T (ATCC, CRL-3216) SW480 (ATCC, CCL-228)
b. Describe the method of cell line authentication used.	All cell lines were purchased at ATCC and authenticated morphologically.
c. Report whether the cell lines were tested for mycoplasma contamination.	Cell lines were tested for mycoplasma contamination.
d. If any of the cell lines used are listed in the database of commonly misidentified cell lines maintained by ICLAC, provide a scientific rationale for their use.	No commonly misidentified cell lines were used.

Animals and human research participants

Policy information about studies involving animals; when reporting animal research, follow the ARRIVE guidelines

11. Description of research animals

Provide details on animals and/or animal-derived materials used in the study.	Mice Tipe2-/- C57BL/6 mice (expressing CD45.2), WT C57BL/6 mice (expressing CD45.1 or CD45.2), males and females. Mice older than 10 weeks were excluded from the study.

Nature Immunology: doi:10.1038/ni.3866

Policy information about studies involving human research participants

12. Description of human research participants

Describe the covariate-relevant population characteristics of the human research participants.	Study did not involve human research participants

Nature Immunology: doi:10.1038/ni.3866